TRANSNAV
http://www.transnav.eu
the International Journal on Marine Navigation and Safety of Sea Transportation
Volume 19
Number 3
September 2025
DOI: 10.12716/1001.19.03.39

Calculation of Free and Forced Lateral Vibrations of a Shaft Line Using Solution Coefficient Vectors

A. Hamiani, K. Boumediene & C. Kandouci
University of Sciences and Technology USTO-MB, Oran, Algeria

ABSTRACT: In this paper, the free and forced lateral vibrations of a marine propulsion shafting system on anisotropic supports are computed using the vectors of solution coefficients method. The transverse vibrations are considered in two orthogonal planes. The effect of the oil film in the bearings is taken into account. The stern tube bearing is considered as an elastic support of Winkler's type. The whirling mode shapes for free vibrations of the system were calculated using the algebraic complements according to I.P. Natanson. The results show a decrease in vertical static deformation due to the distributed weight of the shaft line during the operation of the propelling system. This straightening of the propeller shaft explains the increase in the thickness of the oil film in the stern bearing, as observed by naval engineers.

1 INTRODUCTION

The shaft line performs coupled lateral axial and torsional vibrations under excitation effect generated by the main engine, propeller and ship hull. In theory, when the excitation amplitudes are much larger than the system's dynamic stiffness, resonance effects become dominant, leading to excessive vibrations. Consequently, reducing vibrations and stresses can be achieved by decreasing excitation amplitudes, altering the dominant excitation component, or enhancing the structural dynamic stiffness to shift resonance through a change in the natural frequency.

Forced lateral vibrations from the propulsion shafting system lead to fatigue failure of the bracket and aft stern tube bearing, destruction of high-speed shafts with universal joints, and contribute to noise and hull vibrations [1].The continual increase in propelling power and ship length, the use of high-strength steel, the reduction in wear and corrosion allowances, and the bolder use of lower safety factors lead to an increased disparity between shaft-line stiffness and hull flexibility, and tend to amplify the vibration phenomenon [2]. Lateral vibration may be the cause of dynamic bearing reactions and additional cyclic bending stresses in propeller shaft. Nowadays, all Classification Societies require the propulsion shafting whirling vibration calculation, named in some Class Rules as lateral or bending vibration [1]. Systems are required to operate with acceptable levels of axial bending and torsional vibrations during continuous and transient operating, as stipulated by the makers and pertinent exigence [3]. For all main propulsion shafting systems, shipbuilders must ensure that the lateral vibration characteristics remain satisfactory throughout the entire speed range [4]. In the well-known classification societies DNV [5], we can find rules for vibration analysis of shaft line. These range from the calculation of natural frequencies and forced vibrations, including whirling and axial vibrations, to machinery simulations such as torsional vibration analysis. Zou et al. [6] carried out a dynamic nonlinear-coupled longitudinal-transverse model of a propulsion shafting system and studied the transverse super harmonic resonances under the propeller blade frequency excitation using the method of multiple scales. Busquier et al. [7] considered only the propeller shaft as a self-sustained whirling vibration system and determined its critical speeds by solving the Van der Pol equation. Kim et al. [8] compared the shaft line flexibility and whirling vibration characteristics of double stern tube bearings with those of a single stern tube bearing in a 50000 DWT Oil Tanker. They proposed a new optimum method to provide a satisfactory shaft flexibility in a vessel with a single stern tube bearing, thereby avoiding resonance in whirling vibrations. Qianwen et al. [9] studied the coupled lateral and torsional vibrations under both conditions of idling and loading at different rotational velocity using a finite element model of the marine propulsion shafting system. Zhang et al. [10] studied the dynamic characteristics of the shafting system using a three-DOF transfer matrix-coupling model.Qin H. & al. [11] suggested that incorporating electromagnetic bearings to work in parallel with the rear bearing could effectively reduce lateral vibration transmission. The stern tube bearing sustains the greatest load due to its extended length [12]. The stern tube bearing should be considered as a continuous elastic support at the nominal speed of the propulsion system, whereas the intermediate bearings can be represented as point supports [13]. In this paper, the stern tube bearing is modelled as an elastic support of Winkler's type. The stiffness coefficients of the oil film in the stern tube and intermediate bearings are calculated using the Sommerfeld number. Bending vibrations and static deformations in the horizontal and vertical planes are computed within fixed local coordinate systems using the relationships between the solution coefficient vectors of the governing differential equations. The traditional Transfer Matrix Method (TMM) [14] involves sequentially multiplying transfer matrices, which can lead to numerical instability and computational inefficiency, especially for long shaft lines. However, with the presented approach, the product of multiplied matrices can be represented as a single matrix, when adjacent shaft segments have the same diameters and physical properties, thereby enhancing computational efficiency and numerical stability. From the available literature, we can cite the application of this approach to develop a mathematical model describing linear axial and torsional vibrations of shaft line [15], and to study the whirling vibrations of a shaft carrying three rigid disks resting on rigid supports using the Bernoulli–Euler beam theory [16], and the Timoshenko beam theory [17]. More recently, Kandouci & al. [18] extended this technique to study the whirling vibrations of unbalanced rotor resting on viscoelastic supports.

2 PHYSICAL MODEL OF THE MARINE PROPULSION SHAFTING SYSTEM

Figure 1 provides a physical model of a marine propulsion shafting system made up of n uniform shaft segments [(1), (2), …, (*i*), (*i*+1), …, (*n*-1), (*n*)]. Each shaft segment (*i*) is assigned a length L_i and a fixed coordinate system (x_i, y_i, z_i) with its axes parallel to those of the fixed reference system (*X*, *Y*, *Z*).

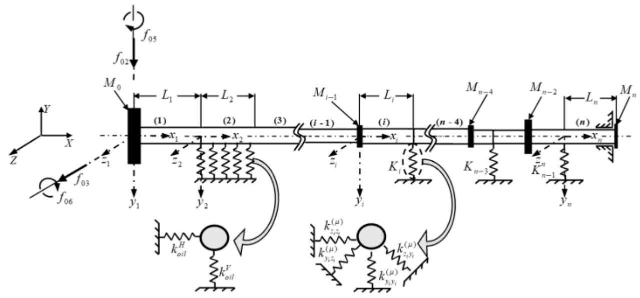

Figure 1. Physical model of the marine propulsion shafting system.

The propeller, coupling flange and sun gear of reduction gearbox are considered to be lumped masses. The division is performed at the junction of two adjacent shaft segments that differ in diameter and/or mechanical properties, at the cross-section passing through the center of gravity of disk (*i*), where shaft segments (*i*) and (*i*+1) connect, and at the end of the *i*-th shaft segment mounted on an elastic support (*i*), such as intermediate bearings and gearbox bearings.

M_0 denotes the propeller inertia matrix, which includes the added mass of seawater, $f_0 = [f_{02}, f_{03}, f_{05}, f_{06}]^T = \{f_{0\alpha}\}$ refers to the vector of hydrodynamic excitations acting on the propeller, α=2 and α=3 correspond to the vertical and horizontal forces, respectively, α=5 and α=6 concern the bending moments in the horizontal and vertical planes, respectively, M_{i-1} and M_{i-4} are the inertia matrices associated with the flange couplings located at the ends of the (*i*-1)th and (*n*-4)th shaft segments, respectively, M_{n-1} and M_n indicate the inertia matrices of the sun gear in the reduction gearbox and the mass at the ends of the (*n*-2)th and *nth* shaft segments, respectively, K_i is the stiffness matrix of the oil film in the intermediate bearing, situated at the end of the *i*th shaft segment, K_{n-3} and K_{n-1} are the stiffness matrices of the oil film in the reduction gearbox bearings, located at the ends of the (*n*-3)th and (*n*-1)th shaft segments, respectively, k^V_{oil} and k^H_{oil} represent the stiffness coefficients of the oil film in the stern tube bearing, modelled as a Winkler-type elastic support, in the vertical and horizontal directions, respectively.

2.1 *Equations of motion*

Neglecting the gyroscopic effect in the shaft, the uncoupled differential equations describing the vertical and horizontal transverse vibrations of the *i*th rotating shaft segment are:

$$\rho_i A_i \frac{\partial^2 w_{i,y}(x,t)}{\partial t^2} + E_i I_{i,z} \frac{\partial^4 w_{i,y}(x,t)}{\partial x^4} = 0 \tag{2.1}$$

$$\rho_i A_i \frac{\partial^2 w_{i,z}(x,t)}{\partial t^2} + E_i I_{y,i} \frac{\partial^4 w_{i,z}(x,t)}{\partial x^4} = 0 \tag{2.2}$$

where $w_{i,y}(x,t)$ and $w_{i,z}(x,t)$ represent the vertical and horizontal transverse vibrations of the cross-sectional centroid of the *i*th shaft segment at the axial coordinate x_i=*x* and time *t*, respectively. $E_i(n/m^2)$ and $\rho_i(kg/m^3)$ are modulus of elasticity and mass density of the *i*th shaft segment. $I_{i,y}(m^4)$ and $I_{i,z}(m^4)$ are diametric moments of inertia of the cross-sectional area A_i about the y_i- or z_i-axis. In the case of a circular shaft, $I_{i,y}=I_{i,z}=I_i$

The vibrations of the shaft segment in the stern bearing (i= 2) are described as follows

$$\rho_2 A_2 \frac{\partial^2 w_{2,y}(x,t)}{\partial t^2} + E_2 I_2 \frac{\partial^4 w_{2,y}(x,t)}{\partial x^4} + k_{oil}^V\ w_{2,y}(x,t) = 0 \qquad (2.3)$$

$$\rho_2 A_2 \frac{\partial^2 w_{2,z}(x,t)}{\partial t^2} + E_2 I_2 \frac{\partial^4 w_{2,z}(x,t)}{\partial x^4} + k_{oil}^H\ w_{2,z}(x,t) = 0 \qquad (2.4)$$

The vibration vector at the axial coordinate x_i=x and time t is designated as:

$$w_i(x,t) = \left[w_{i,y}(x,t), w_{i,z}(x,t), \theta_{i,y}(x,t), \theta_{i,z}(x,t) \right]^T$$

The rotational vibrations, bending moment and shear forces, as described by Bernoulli–Euler beam theory, are expressed as follows:

$$\theta_{i,y}(x,t) = -\frac{\partial w_{i,z}(x,t)}{\partial x}, \quad \theta_{i,z}(x,t) = \frac{\partial w_{i,y}(x,t)}{\partial x} \qquad (2.5)$$

$$Q_{i,y}(x,t) = -E_i I_i \frac{\partial^3 w_{i,y}(x,t)}{\partial x^3}, \quad Q_{i,z}(x,t) = -E_i I_i \frac{\partial^3 w_{i,z}(x,t)}{\partial x^3} \qquad (2.6)$$

$$M_{i,y}(x,t) = E_i I_i \frac{\partial^2 w_{i,z}(x,t)}{\partial x^2}, \quad M_{i,z}(x,t) = -E_i I_i \frac{\partial^2 w_{i,y}(x,t)}{\partial x^2} \qquad (2.7)$$

The internal force and moment vector at axial coordinate x_i=x and time t is expressed as:

$$p_i(x,t) = \left[Q_{i,y}(x,t), Q_{i,z}(x,t), M_{i,y}(x,t), M_{i,z}(x,t) \right]^T$$

The propulsion shafting system's boundary conditions at its left and right ends, as illustrated in Figure 1, are expressed as follows:

$$-p_1(0,t) + \bar{E}\left(M_0 \ddot{w}_1(0,t) + \Pi \dot{w}_1(0,t) \right) = \bar{E} f_0 \qquad (2.8)$$

$$-p_n(L_n,t) - \bar{E} M_n \ddot{w}_n(L_n,t) = 0 \qquad (2.9)$$

where M_0=M_p+M_w, M_p is the inertia matrix of the propeller, M_w denotes the inertia matrix of the added water mass,

$$M_p = diag(m_p,\ m_p,\ J_d,\ J_d),\ \bar{E} = diag(1,\ 1,\ -1,\ -1)$$

$$M_w = \begin{bmatrix} m_{22} & -m_{32} & m_{52} & -m_{62} \\ m_{32} & m_{33} & m_{62} & m_{52} \\ m_{52} & -m_{62} & m_{55} & -m_{65} \\ m_{62} & m_{52} & m_{65} & m_{55} \end{bmatrix}$$

m_p and J_d represent the mass and diametrical mass moment of inertia of the propeller under dry conditions.

$$\Pi = \Pi_g + \Pi_w$$

$$\Pi_g = \begin{bmatrix} 0 & 0 & 0 & 0 \\ 0 & 0 & 0 & 0 \\ 0 & 0 & -\Omega J_{xx} & 0 \\ 0 & 0 & 0 & \Omega J_{xx} \end{bmatrix}, \quad \Pi_w = \begin{bmatrix} c_{22} & -c_{32} & c_{52} & -c_{62} \\ c_{32} & c_{33} & c_{62} & c_{52} \\ c_{52} & -c_{62} & c_{55} & -c_{65} \\ c_{62} & c_{52} & c_{65} & c_{55} \end{bmatrix}$$

Π_g and Π_w denote the matrices of gyroscopic moments induced in the propeller and viscous damping coefficients, respectively. J_{xx} is the propeller polar moment of inertia about the shaft axis. The added mass and damping matrices, (M_w and Π_w), are calculated using the relationships given by Carlton [19].

The hydrodynamic excitations acting on the propeller rotating at speed ω are expressed in terms of a Fourier series as follows

$$f_{0\alpha} = f_{0\alpha}^{(0)} + \sum_{\mu} f_{0\alpha}^{(\mu)} \cos\left(\nu\omega t + \varphi_{0\alpha}^{(\mu)} \right),\ (\mu = 1,2,...),\ (\alpha\text{=2,3,5,6}) \qquad (2.10)$$

where $\bar{f}_{0\alpha}^{(\mu)}$ is the complex amplitude defined as

$$\bar{f}_{0\alpha}^{(\mu)} = \hat{f}_{0\alpha}^{(\mu)} e^{i\varphi_{0\alpha}^{(\mu)}}, \quad \left(\mu = 1,2,... \right),\ \left(\alpha\text{=2,3,5,6} \right) \qquad (2.11)$$

In the above equation, $\hat{f}_{0\alpha}^{(\mu)}$ and $\varphi_{0\alpha}^{(\mu)}$ represent the real amplitude and initial phase of the μth component of the hydrodynamic excitation in the directionα, (α=2, 3, 5, 6) at propeller angular velocityω.

The vibrations can be found as the real parts of the following expressions

$$w_{i,y}(x,t) = \sum_{\mu} \bar{w}_{i,y}^{(\mu)}(x) e^{j\mu\omega t}, \qquad w_{i,z}(x,t) = \sum_{\mu} \bar{w}_{i,z}^{(\mu)}(x) e^{j\mu\omega t} \qquad (2.12)$$

$$\theta_{i,y}(x,t) = \sum_{\mu} \bar{\theta}_{i,y}^{(\mu)}(x) e^{j\mu\omega t}, \qquad \theta_{i,z}(x,t) = \sum_{\mu} \bar{\theta}_{i,z}^{(\mu)}(x) e^{j\mu\omega t} \qquad (2.13)$$

Substituting Eq. (2.12) into differential Eqs. (2.1) and (2.2) yields

$$w_i(x,t) = \sum_{\mu} \bar{w}_i^{(\mu)}(x) e^{j\mu\omega t}, \qquad \mu = 0,1,2,... \qquad (2.14)$$

$$p_i(x,t) = \sum_{\mu} \bar{p}_i^{(\mu)}(x) e^{j\mu\omega t} \qquad \mu = 0,1,2,... \qquad (2.15)$$

$$\bar{u}_i^{(\mu)}(x) = C_i^{(\mu)}(x) a_i^{(\mu)} \qquad (2.16)$$

$$\bar{p}_i^{(\mu)}(x) = D_i^{(\mu)}(x) a_i^{(\mu)} \qquad (2.17)$$

In Eqs. (2.16) and (2.17), $a_i^{(\mu)} = \left\{ a_{iq}^{(\mu)} \right\},\ q = 1,2,...,8$ is the vector of solution coefficients for the ith shaft segment, and it can be determined using the continuity of displacements, equilibrium of forces (and moments) as well as boundary conditions (2.8) and (2.9). While:

– for μ=0 and i≠2, we get

$$C_i^{(0)}(x) = \begin{bmatrix} x^3 & x^2 & x & 1 & 0 & 0 & 0 & 0 \\ 0 & 0 & 0 & 0 & x^3 & x^2 & x & 1 \\ 0 & 0 & 0 & 0 & -3x^2 & -2x & -1 & 0 \\ 3x^2 & 2x & 1 & 0 & 0 & 0 & 0 & 0 \end{bmatrix}$$

$$D_i^{(0)}(x) = EI \begin{bmatrix} -6 & 0 & 0 & 0 & 0 & 0 & 0 & 0 \\ 0 & 0 & 0 & 0 & -6 & 0 & 0 & 0 \\ 0 & 0 & 0 & 0 & 6x & 2 & 0 & 0 \\ -6x & -2 & 0 & 0 & 0 & 0 & 0 & 0 \end{bmatrix}$$

– for $\mu\neq0$ and $i\neq2$, we obtain
$C_i^{(\mu)}(x)=\left[\left(C_i^{(\mu)}(x)\right)_1:\left(C_i^{(\mu)}(x)\right)_2\right]$ and
$D_i^{(\mu)}(x)=\left[\left(D_i^{(\mu)}(x)\right)_1:\left(D_i^{(\mu)}(x)\right)_2\right]$,

where

$$\left(C_i^{(\mu)}(x)\right)_1=\begin{bmatrix}\cos\beta x & \sin\beta x & ch\beta x & sh\beta x\\ 0&0&0&0\\ 0&0&0&0\\ -\beta\sin\beta x & \beta\cos\beta x & \beta sh\beta x & \beta ch\beta x\end{bmatrix},$$

$$\left(C_i^{(\mu)}(x)\right)_2=\begin{bmatrix}0&0&0&0\\ \cos\beta x & \sin\beta x & ch\beta x & sh\beta x\\ \beta\sin\beta x & -\beta\cos\beta x & -\beta sh\beta x & -\beta ch\beta x\\ 0&0&0&0\end{bmatrix}$$

$$\left(D_i^{(\mu)}(x)\right)_1=EI\begin{bmatrix}-\beta^3\sin\lambda x & \beta^3\cos\beta x & -\beta^3 sh\beta x & -\beta^3 ch\beta x\\ 0&0&0&0\\ 0&0&0&0\\ \beta^2\cos\beta x & \beta^2\sin\beta x & -\beta^2 ch\beta x & -\beta^2 sh\beta x\end{bmatrix},$$

$$\left(D_i^{(\mu)}(x)\right)_2=EI\begin{bmatrix}0&0&0&0\\ -\beta^3\sin\beta x & \beta^3\cos\beta x & -\beta^3 sh\beta x & -\beta^3 ch\beta x\\ -\beta^2\cos\beta x & -\beta^2\sin\beta x & \beta^2 ch\beta x & \beta^2 sh\beta x\\ 0&0&0&0\end{bmatrix}$$

with $\beta=\beta^{(\mu)}=[\mu^2\omega^2A_i\rho_i/(E_iI_i)]^{1/4}$

For the shaft segment in the stern tube bearing (i =2), the substitution of Eq. (2.12) into differential Eqs. (2.3) and (2.4) leads to

$$u_2(x,t)=\sum_\mu\bar{u}_2^{(\mu)}(x)e^{j\mu\omega t},\qquad \mu=0,1,2,... \tag{2.18}$$

$$p_2(x,t)=\sum_\mu\bar{p}_2^{(\mu)}(x)e^{j\mu\omega t}\qquad \mu=0,1,2,... \tag{2.19}$$

$$\bar{u}_2^{(\mu)}(x)=C_2^{(\mu)}(x)a_2^{(\mu)} \tag{2.20}$$

$$\bar{p}_2^{(\mu)}(x)=D_2^{(\mu)}(x)a_2^{(\mu)} \tag{2.21}$$

where
– for μ=0, we get $C_2^{(\mu)}(x)=\left[\left(C_2^{(\mu)}(x)\right)_1:\left(C_2^{(\mu)}(x)\right)_2\right]$ and $D_2^{(\mu)}(x)=\left[\left(D_2^{(\mu)}(x)\right)_1:\left(D_2^{(\mu)}(x)\right)_2\right]$,

where

$$\left(C_2^{(0)}(x)\right)_1=\begin{bmatrix}Q_V & N_V & S_V & T_V\\ 0&0&0&0\\ 0&0&0&0\\ \beta_V(S_V-N_V) & \beta_V(Q_V-T_V) & \beta_V(Q_V+T_V) & \beta_V(N_V+S_V)\end{bmatrix},$$

$$\left(C_2^{(0)}(x)\right)_2=\begin{bmatrix}0&0&0&0\\ Q_H & N_H & S_H & T_H\\ \beta_H(S_H-N_H) & \beta_H(T_H-Q_H) & -\beta_H(Q_H+T_H) & -\beta_H(N_H+S_H)\\ 0&0&0&0\end{bmatrix},$$

$$\left(D_{2x}^{(0)}\right)_1=2EI\begin{bmatrix}\beta_V^3(N_V+S_V) & \beta_V^3(Q_V+T_V) & \beta_V^3(T_V-Q_V) & \beta_V^3(S_V-N_V)\\ 0&0&0&0\\ 0&0&0&0\\ \beta_V^2T_V & \beta_V^2S_V & -\beta_V^2N_V & -\beta_V^2Q_V\end{bmatrix},$$

$$\left(D_{2x}^{(0)}\right)_2=2EI\begin{bmatrix}0&0&0&0\\ \beta_H^3(N_H+S_H) & \beta_H^3(Q_H+T_H) & \beta_H^3(T_H-Q_H) & \beta_H^3(S_H-N_H)\\ -\beta_H^2T_H & -\beta_H^2S_H & \beta_H^2N_H & \beta_H^2Q_H\\ 0&0&0&0\end{bmatrix},$$

with

$Q_V=\cos(\beta_Vx)\,ch(\beta_Vx)$, $N_V=\cos(\beta_Vx)\,sh(\beta_Vx)$,
$S_V=\sin(\beta_Vx)\,ch(\beta_Vx)$, $T_V=\sin(\beta_Vx)\,sh(\beta_Vx)$.
$Q_H=\cos(\beta_Hx)\,ch(\beta_Hx)$, $N_H=\cos(\beta_Hx)\,sh(\beta_Hx)$,
$S_H=\sin(\beta_Hx)\,ch(\beta_Hx)$, $T_H=\sin(\beta_Hx)\,sh(\beta_Hx)$,
$\beta_V=\left(k_{oil}^V/4E_2I_2\right)^{1/4}$, *and* $\beta_H=(k_{oil}^H/4E_2I_2)^{1/4}$.

For $\mu\neq0$, four cases that can be encountered for the shaft segment in the stern tube bearing, (i =2):

A- if $(k_{oil}^{V(\mu)}-\mu^2\omega^2\rho_2A_2)<0$ and $(k_{oil}^{H(\mu)}-\mu^2\omega^2\rho_2A_2)<0$, we obtain
$C_2^{(\mu)}(x)=\left[\left(C_2^{(\mu)}(x)\right)_1:\left(C_2^{(\mu)}(x)\right)_2\right]$ and
$D_2^{(\mu)}(x)=\left[\left(D_2^{(\mu)}(x)\right)_1:\left(D_2^{(\mu)}(x)\right)_2\right]$,
where

$$\left(C_2^{(\mu)}(x)\right)_1=\begin{bmatrix}\cos\beta_{V^-}x & \sin\beta_{V^-}x & ch\beta_{V^-}x & sh\beta_{V^-}x\\ 0&0&0&0\\ 0&0&0&0\\ -\beta_{V^-}\sin\beta_{V^-}x & \beta_{V^-}\cos\beta_{V^-}x & \beta_{V^-}sh\beta_{V^-}x & \beta_{V^-}ch\beta_{V^-}x\end{bmatrix},$$

$$\left(C_2^{(\mu)}(x)\right)_2=\begin{bmatrix}0&0&0&0\\ \cos\beta_{H^-}x & \sin\beta_{H^-}x & ch\beta_{H^-}x & sh\beta_{H^-}x\\ \beta_{H^-}\sin\beta_{H^-}x & -\beta_{H^-}\cos\beta_{H^-}x & -\beta_{H^-}sh\beta_{H^-}x & -\beta_{H^-}ch\beta_{H^-}x\\ 0&0&0&0\end{bmatrix},$$

$$\left(D_2^{(\mu)}(x)\right)_1=EI\begin{bmatrix}-\beta_{V^-}^3\sin\beta_{V^-}x & \beta_{V^-}^3\cos\beta_{V^-}x & -\beta_{V^-}^3sh\beta_{V^-}x & -\beta_{V^-}^3ch\beta_{V^-}x\\ 0&0&0&0\\ 0&0&0&0\\ \beta_{V^-}^2\cos\beta_{V^-}x & \beta_{V^-}^2\sin\beta_{V^-}x & -\beta_{V^-}^2ch\beta_{V^-}x & -\beta_{V^-}^2sh\beta_{V^-}x\end{bmatrix},$$

$$\left(D_2^{(\mu)}(x)\right)_2=EI\begin{bmatrix}0&0&0&0\\ -\beta_{H^-}^3\sin\beta_{H^-}x & \beta_{H^-}^3\cos\beta_{H^-}x & -\beta_{H^-}^3sh\beta_{H^-}x & -\beta_{H^-}^3ch\beta_{H^-}x\\ -\beta_{H^-}^2\cos\beta_{H^-}x & -\beta_{H^-}^2\sin\beta_{H^-}x & \beta_{H^-}^2ch\beta_{H^-}x & \beta_{H^-}^2sh\beta_{H^-}x\\ 0&0&0&0\end{bmatrix},$$

with

$\beta_{V^-}=\beta_{V^-}^{(\mu)}=\left[(\mu^2\omega^2\rho_2A_2-k_{oil}^V)/(E_2I_2)\right]^{1/4}$ and
$\beta_{H^-}=\beta_{H^-}^{(\mu)}=\left[(\mu^2\omega^2\rho_2A_2-k_{oil}^H)/(E_2I_2)\right]^{1/4}$.

B- If $(k_{oil}^{V(\mu)}-\mu^2\omega^2\rho_2A_2)>0$ and $(k_{oil}^{H(\mu)}-\mu^2\omega^2\rho_2A_2)>0$, we get $C_2^{(\mu)}(x)=\left[\left(C_2^{(\mu)}(x)\right)_1:\left(C_2^{(\mu)}(x)\right)_2\right]$ and
$D_2^{(\mu)}(x)=\left[\left(D_2^{(\mu)}(x)\right)_1:\left(D_2^{(\mu)}(x)\right)_2\right]$,
where

$$\left(C_2^{(\mu)}(x)\right)_1=\begin{bmatrix}Q_{V^+} & N_{V^+} & S_{V^+} & T_{V^+}\\ 0&0&0&0\\ 0&0&0&0\\ \beta_{V^+}(N_{V^+}-S_{V^+}) & \beta_{V^+}(Q_{V^+}-T_{V^+}) & \beta_{V^+}(Q_{V^+}+T_{V^+}) & \beta_{V^+}(N_{V^+}+S_{V^+})\end{bmatrix},$$

$$\left(C_2^{(\mu)}(x)\right)_2=\begin{bmatrix}0&0&0&0\\ Q_{H^+} & N_{H^+} & S_{H^+} & T_{H^+}\\ \beta_{H^+}(S_{H^+}-N_{H^+}) & \beta_{H^+}(T_{H^+}-Q_{H^+}) & -\beta_{H^+}(Q_{H^+}+T_{H^+}) & -\beta_{H^+}(N_{H^+}+S_{H^+})\\ 0&0&0&0\end{bmatrix},$$

$$\left(D_{2x}^{(\mu)}\right)_1=2EI\begin{bmatrix}\beta_{V^+}^3\left(N_{V^+}+S_{V^+}\right) & \beta_{V^+}^3\left(Q_{V^+}+T_{V^+}\right) & \beta_{V^+}^3\left(T_{V^+}-Q_{V^+}\right) & \beta_{V^+}^3\left(S_{V^+}-N_{V^+}\right)\\ 0&0&0&0\\ 0&0&0&0\\ \beta_{V^+}^2T_{V^+} & \beta_{V^+}^2S_{V^+} & -\beta_{V^+}^2N_{V^+} & -\beta_{V^+}^2Q_{V^+}\end{bmatrix},$$

$$\left(D_{2x}^{(\mu)}\right)_2=2EI\begin{bmatrix}0&0&0&0\\ \beta_{H^+}^3\left(N_{H^+}+S_{H^+}\right) & \beta_{H^+}^3\left(Q_{H^+}+T_{H^+}\right) & \beta_{H^+}^3\left(T_{H^+}-Q_{H^+}\right) & \beta_{H^+}^3\left(N_{H^+}-S_{H^+}\right)\\ -\beta_{H^+}^2T_{H^+} & -\beta_{H^+}^2S_{H^+} & \beta_{H^+}^2N_{H^+} & \beta_{H^+}^2Q_{H^+}\\ 0&0&0&0\end{bmatrix},$$

with

$Q_{V^+} = \cos(\beta_{V^+}x)\, ch(\beta_{V^+}x),\; N_{V^+} = \cos(\beta_{V^+}x) sh(\beta_{V^+}x),$
$S_{V^+} = \sin(\beta_{V^+}x) ch(\beta_{V^+}x),\; T_{V^+} = \sin(\beta_{V^+}x) sh(\beta_{V^+}x),$
$Q_{H^+} = \cos(\beta_{H^+}x) ch(\beta_{H^+}x),\; N_{H^+} = \cos(\beta_{H^+}x) sh(\beta_{H^+}x),$
$S_{H^+} = \sin(\beta_{H^+}x) ch(\beta_{H^+}x),\; T_{H^+} = \sin(\beta_{H^+}x) sh(\beta_{H^+}x),$
$\beta_{V^+} = \beta_{V^+}^{(\mu)} = \left[(k_{Oil}^{V} - \mu^2\omega^2\rho_2 A_2)/(4E_2 I_2)\right]^{1/4}$, and
$\beta_{H^+} = \beta_{H^+}^{(\mu)} = \left[(k_{oil}^{H} - \mu^2\omega^2\rho_2 A_2)/(4E_2 I_2)\right]^{1/4}$

C- If $(k_{oil}^{V^{(\mu)}} - \mu^2\omega^2\rho_2 A_2) < 0$ and $(k_{oil}^{H^{(\mu)}} - \mu^2\omega^2\rho_2 A_2) > 0$, we obtain

$C_2^{(\mu)}(x) = \left[\left(C_2^{(\mu)}(x)\right)_1 : \left(C_2^{(\mu)}(x)\right)_2\right]$ and
$D_2^{(\mu)}(x) = \left[\left(D_2^{(\mu)}(x)\right)_1 : \left(D_2^{(\mu)}(x)\right)_2\right],$

with $\left(C_2^{(\mu)}(x)\right)_1$ and $\left(D_2^{(\mu)}(x)\right)_1$ as in case A, while $\left(C_2^{(\mu)}(x)\right)_2$ and $\left(D_2^{(\mu)}(x)\right)_2$ as in case B,

D- If $(k_{oil}^{V^{(\mu)}} - \mu^2\omega^2\rho_2 A_2) > 0$ and $(k_{oil}^{H^{(\mu)}} - \mu^2\omega^2\rho_2 A_2) < 0$, we get $C_2^{(\mu)}(x) = \left[\left(C_2^{(\mu)}(x)\right)_1 : \left(C_2^{(\mu)}(x)\right)_2\right]$ and $D_2^{(\mu)}(x) = \left[\left(D_2^{(\mu)}(x)\right)_1 : \left(D_2^{(\mu)}(x)\right)_2\right]$, with $\left(C_2^{(\mu)}(x)\right)_1$ and $\left(D_2^{(\mu)}(x)\right)_1$ as in case B, while, $\left(C_2^{(\mu)}(x)\right)_2$ and $\left(D_2^{(\mu)}(x)\right)_2$ as in case A.

2.2 *Transfer matrices related to the solution coefficient vectors for different adjacent shaft segments*

A junction between two adjacent shaft segments, (i) and (i+1), is shown in Figure 2. The axes x_i, y_i, z_i of the ith shaft segment are parallel to the axes X, Y, Z of the fixed local coordinate system, as illustrated in Figure 1. The length of the ith shaft segment is denoted by L_i

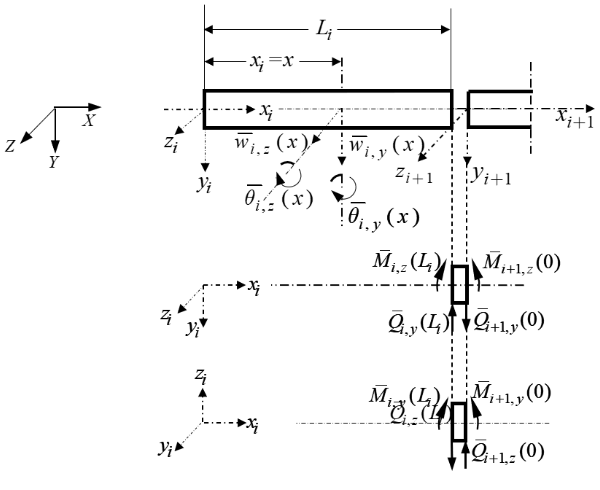

Figure 2. Schematic illustration of displacements, slopes, shear forces and bending moments acting at junction of two adjacent shaft segments (i) and (i+1), with different diameters and/or physical properties.

2.2.1 *Case of shaft segments (i) and (i+1) with different mechanical properties and/or diameters*

The continuity of displacements and the equilibrium of shearing forces and bending moments, at a junction of two shaft segments, (i) and (i+1), with different mechanical properties and/or diameters require that

$$\bar{w}_i^{(\mu)}(L_i) = \bar{w}_{i+1}^{(\mu)}(0) \tag{2.22}$$

$$\bar{p}_i^{(\mu)}(L_i) = \bar{p}_{i+1}^{(\mu)}(0) \tag{2.23}$$

Taking into account Eqs. (2.14-2.17), the conditions (2.22) and (2.23) can be expressed in the following form

$$C_i^{(\mu)}(L_i) a_i^{(\mu)} = C_{i+1}^{(\mu)}(0) a_{i+1}^{(\mu)} \tag{2.24}$$

$$D_i^{(\mu)}(L_i) a_i^{(\mu)} = D_{i+1}^{(\mu)}(0) a_{i+1}^{(\mu)} \tag{2.25}$$

$$a_{i+1}^{(\mu)} = B_i^{(\mu)} a_i^{(\mu)} \tag{2.26}$$

$$B_i^{(\mu)} = \begin{bmatrix} C_{i+1}^{(\mu)}(0) \\ D_{i+1}^{(\mu)}(0) \end{bmatrix}^{-1} \begin{bmatrix} C_i^{(\mu)}(L_i) \\ D_i^{(\mu)}(L_i) \end{bmatrix} \tag{2.27}$$

where $B_i^{(\mu)}$ is a block diagonal matrix,

$$B_i^{(\mu)} = \begin{bmatrix} B_{i2}^{(\mu)} & 0 \\ 0 & B_{i3}^{(\mu)} \end{bmatrix},\quad B_{i2}^{(0)} = B_{i3}^{(0)} = \begin{bmatrix} \frac{E_i I_i}{E_{i+1} I_{i+1}} & 0 & 0 & 0 \\ \frac{3E_i I_i}{E_{i+1} I_{i+1}} & \frac{E_i I_i}{E_{i+1} I_{i+1}} & 0 & 0 \\ 3L_i^2 & 2L_i & 1 & 0 \\ L_i^3 & L_i^2 & L_i & 1 \end{bmatrix} \tag{2.28}$$

$$^{+}B_{i1}^{(\mu)} = B_{i2}^{(\mu)} = \begin{bmatrix} \xi_1^{(\mu)}\cos(\beta l) & \xi_1^{(\mu)}\sin(\beta l) & \xi_2^{(\mu)} ch(\beta l) & \xi_2^{(\mu)} sh(\beta l) \\ -\xi_3^{(\mu)}\sin(\beta l) & \xi_3^{(\mu)}\cos(\beta l) & \xi_4^{(\mu)} sh(\beta l) & \xi_4^{(\mu)} ch(\beta l) \\ \xi_2^{(\mu)}\cos(\beta l) & \xi_2^{(\mu)}\sin(\beta l) & \xi_1^{(\mu)} ch(\beta l) & \xi_1^{(\mu)} sh(\beta l) \\ -e_4^{(\mu)}\sin(\beta l) & e_4^{(\mu)}\cos(\beta l) & \xi_3^{(\mu)} sh(\beta l) & \xi_3^{(\mu)} ch(\beta l) \end{bmatrix}_{(i)} \tag{2.29}$$

$$\left(\xi_1^{(\mu)}\right)_i = \frac{1}{2} + \frac{E_i I_i \beta_i^2}{2E_{i+1} I_{i+1} \beta_{i+1}^2},\qquad \left(\xi_2^{(\mu)}\right)_i = \frac{1}{2} - \frac{E_i I_i \beta_i^2}{2E_{i+1} I_{i+1} \beta_{i+1}^2},$$
$$\left(\xi_3^{(\mu)}\right)_i = \frac{\beta_i}{2\beta_{i+1}} + \frac{E_i I_i \beta_i^3}{2E_{i+1} I_{i+1} \beta_{i+1}^3},\quad \left(\xi_4^{(\mu)}\right)_i = \frac{\beta_i}{2\beta_{i+1}} - \frac{E_i I_i \beta_i^3}{2E_{i+1} I_{i+1} \beta_{i+1}^3} \tag{2.30}$$

Thus, the relationships between the vectors of solution coefficients $a_i^{(\mu)}$ and $a_{i+1}^{(\mu)}$ are written in matrix form. For the (r-1) following shaft segments, we have the relationship:

$$a_{i+r}^{(\mu)} = B_{i+r-1}^{(\mu)} B_{i+r-2}^{(\mu)} \ldots B_i^{(\mu)} a_i^{(\mu)} \tag{2.31}$$

For long shaft line vibration, the number of multiplied matrices in Eq. (2.31) may be large, however, compared with the classical transfer matrix method (TMM), the matrices $B_i^{(\mu)}$ present an advantageous property for shaft segments with the same mechanical and geometric properties, that reduces the number of multiplied matrix product in Eq. (2.31) to a single matrix as follows

$$a_{i+s}^{(\mu)} = \mathrm{T}_i^{(\mu)} a_i^{(\mu)} \tag{2.32}$$

where the matrix $\mathrm{T}_i^{(\mu)}$ is obtained from the matrix $B_i^{(\mu)}$ by setting $\left(\xi_1^{(\mu)}\right)_i = \left(\xi_3^{(\mu)}\right)_i = 1$, $\left(\xi_2^{(\mu)}\right)_i = \left(\xi_4^{(\mu)}\right)_i = 0$ and replacing L_i by

$$L_i = \sum_{p=i}^{p=i+r-1} L_p \tag{2.33}$$

The matrix $\mathrm{T}_i^{(\mu)}$ can be understood as a transfer matrix associated with the solution coefficient vectors $a_i^{(\mu)}$ and $a_{i+1}^{(\mu)}$. However, it should not be confused with the transfer matrix commonly used in the well-known Transfer Matrix Method (TMM).

2.2.2 *Case of adjacent shaft segments (i) and (i+1) joined by a discrete mass mi*

When the section connecting two adjacent shaft segments, (*i*) and (*i*+1), passes through a gravity center of discrete mass m_i with a diametrical mass moment of inertia J_i (e.g. flange coupling, sun gear of reduction gear box), the continuity of displacements and the equilibrium of forces (and moments) require that

$$\bar{w}_i^{(\mu)}(L_i) = \bar{w}_{i+1}^{(\mu)}(0) \tag{2.34}$$

$$\bar{p}_i^{(\mu)}(L_i) = \bar{p}_{i+1}^{(\mu)}(0) + \omega^2 M_i \bar{w}_i^{(\mu)}(L_i) \tag{2.35}$$

where M_i is the diagonal inertia matrix of the discrete mass m_i located at the end of the *i*th shaft segment $M_i = diag(m_i,\ m_i,\ J_i,\ J_i)$

Equations (2.34) and (2.35) can be expressed as

$$C_i^{(\mu)}(L_i) a_i^{(\mu)} = C_{i+1}^{(\mu)}(0) a_{i+1}^{(\mu)} \tag{2.36}$$

$$D_i^{(\mu)}(L_i) a_i^{(\mu)} = D_{i+1}^{(\mu)}(0) a_{i+1}^{(\mu)} + \omega^2 M_i C_i^{(\mu)}(L_i) a_i^{(\mu)} \tag{2.37}$$

Thus, the relationships between the solution coefficient vectors $a_i^{(\mu)}$ and $a_{i+1}^{(\mu)}$, for two shaft segments joined at a discrete mass, can be formulated in a matrix form as

$$a_{i+1}^{(\mu)} = R_i^{(\mu)} a_i^{(\mu)} \tag{2.38}$$

where

$$R_i^{(\mu)} = \begin{bmatrix} C_{i+1}^{(\mu)}(0) \\ D_{i+1}^{(\mu)}(0) \end{bmatrix}^{-1} \begin{bmatrix} C_i^{(\mu)}(L_i) \\ D_i^{(\mu)}(L_i) - \omega^2 M_i C_i^{(\mu)}(L_i) \end{bmatrix} \tag{2.39}$$

$R_i^{(\mu)}$ serves as the transfer matrix that relates the solution coefficient vectors $a_i^{(\mu)}$ and $a_{i+1}^{(\mu)}$ via mass (*i*).

2.2.3 *Case of intermediary anisotropic supporting bearing*

In such a case, the continuity of deformations and equilibrium of internal forces and moments require that

$$\bar{w}_i^{(\mu)}(L_i) = \bar{w}_{i+1}^{(\mu)}(0) \tag{2.40}$$

$$\bar{p}_i^{(\mu)}(L_i) = \bar{p}_{i+1}^{(\mu)}(0) + \bar{E} K_i \bar{u}_i^{(\mu)}(L_i) \tag{2.41}$$

where K_i is the stiffness matrix of the oil film in the *i*th intermediate bearing, defined as follows

$$K_i = \begin{bmatrix} k_{22} & k_{23} & 0 & 0 \\ k_{32} & k_{33} & 0 & 0 \\ 0 & 0 & 0 & 0 \\ 0 & 0 & 0 & 0 \end{bmatrix}$$

The equations (2.40) and (2.41) can be expressed in the following form

$$C_i^{(\mu)}(L_i) a_i^{(\mu)} = C_{i+1}^{(\mu)}(0) a_{i+1}^{(\mu)} \tag{2.42}$$

$$D_i^{(\mu)}(L_i) a_i^{(\mu)} = D_{i+1}^{(\mu)}(0) a_{i+1}^{(\mu)} - \bar{E} K_i C_i^{(\mu)}(L_i) a_i^{(\mu)} \tag{2.43}$$

Writing Eqs. (2.42) and (2.43) in matrix form produces

$$a_{i+1}^{(\mu)} = S_i^{(\mu)} a_i^{(\mu)} \tag{2.44}$$

where

$$S_i^{(\mu)} = \begin{bmatrix} C_{i+1}^{(\mu)}(0) \\ D_{i+1}^{(\mu)}(0) \end{bmatrix}^{-1} \begin{bmatrix} C_i^{(\mu)}(L_i) \\ D_i^{(\mu)}(L_i) + \bar{E} K_i C_i^{(\mu)}(L_i) \end{bmatrix} \tag{2.45}$$

where $S_i^{(\mu)}$ is the transfer matrix through the intermediate bearing (i).

Using the above relationships between different adjacent shaft segments, the vectors of solution coefficient $a_2^{(\mu)},\ a_3^{(\mu)}, \ldots,\ a_n^{(\mu)}$ for the vibrations from the second to the nth shaft segment can be determined, as function of $a_1^{(\mu)}$, which represents the coefficient vector for lateral vibrations of the first shaft segment. For the system as shown in Figure 1, we get

$$\begin{aligned} a_2^{(\mu)} &= B_1^{(\mu)} a_1^{(\mu)}, \\ a_3^{(\mu)} &= B_2^{(\mu)} B_1^{(\mu)} a_1^{(\mu)}, \\ a_4^{(\mu)} &= R_3^{(\mu)} B_2^{(\mu)} B_1^{(\mu)} a_1^{(\mu)}, \\ a_5^{(\mu)} &= S_4^{(\mu)} R_3^{(\mu)} B_2^{(\mu)} B_1^{(\mu)} a_1^{(\mu)}, \\ &\vdots \\ a_n^{(\mu)} &= B_{n-1}^{(\mu)} \ldots S_4^{(\mu)} R_3^{(\mu)} B_2^{(\mu)} B_1^{(\mu)} a_1^{(\mu)}. \end{aligned} \tag{2.46}$$

3 FREE VIBRATION ANALYSIS

Similarly, the boundary conditions (2.8) and (2.9) can be written in the following matrix

$$\Gamma \left\{ a_1^{(\mu)} \right\} = \begin{Bmatrix} \bar{E} \bar{f}_0^{(\mu)} \\ 0 \end{Bmatrix} \tag{3.1}$$

where

$$\Gamma = \begin{bmatrix} \Gamma_{11} & \Gamma_{12} & \cdots & \Gamma_{18} \\ \Gamma_{21} & \cdots & & \\ \vdots & \cdots & & \\ \Gamma_{81} & \cdots & & \Gamma_{88} \end{bmatrix} = \begin{bmatrix} -D_{1,0}^{(\mu)} + \left[j\mu\omega c_0^{(\mu)} - (\mu\omega)^2 \bar{E} M_0 \right] C_{1,0}^{(\mu)} \\ \left[-D_n^{(\mu)}(L_n) + (\mu\omega)^2 \bar{E} M_n C_n^{(\mu)}(L_n) \right] B_{n-1}^{(\mu)} \ldots\ldots B_5^{(\mu)} S_4^{(\mu)} R_3^{(\mu)} B_2^{(\mu)} B_1^{(\mu)} \end{bmatrix} \tag{3.2}$$

with $\left\{ a_1^{(\mu)} \right\} = \left[a_{1,1}^{(\mu)},\ a_{1,2}^{(\mu)},\ a_{1,3}^{(\mu)}\ \ldots\ a_{1,8}^{(\mu)} \right]^T$.

3.1 *Natural frequencies and associated mode shapes*

For μ=1, free vibrations occur when $\bar{f}_0^{(1)} = 0$, and the characteristic equation is given by

$$\Gamma . \left\{ a_1^{(1)} \right\} = 0 \tag{3.3}$$

with $\left\{ a_1^{(1)} \right\} = \left[a_{1,1}^{(1)},\ a_{1,2}^{(1)},\ a_{1,3}^{(1)}\ \ldots\ a_{1,8}^{(1)} \right]^T$.

Nontrivial solution for the column vector $a_1^{(1)}$, requires that

$$|\Gamma| = 0 \tag{3.4}$$

The natural frequencies for the non-rotating shaft line may be obtained by solving the above eigenvalue equation (3.4). For each value of natural frequency, the matrix Γ in equation (3.4) is singular. In such cases, Natanson's technique [20], which use the algebraic complements, can be applied to determine the eigenvector for the first shaft segment, up to a multiplicative constant ϕ:

$$a_{1,1}^{(1)} = \phi.\Lambda_{1,1},\ \ a_{1,2}^{(1)} = \phi.\Lambda_{1,2},\ \ \dots\ \ ,\ a_{1,8}^{(1)} = \phi.\Lambda_{1,8} \tag{3.5}$$

$$\Lambda_{11} = \begin{vmatrix} \Gamma_{22} & \Gamma_{23} & \cdots & \Gamma_{28} \\ \Gamma_{32} & \cdots & & \\ \vdots & \cdots & & \\ \Gamma_{82} & \cdots & & \Gamma_{88} \end{vmatrix},\ \ \Lambda_{12} = -\begin{vmatrix} \Gamma_{21} & \Gamma_{23} & \cdots & \Gamma_{28} \\ \Gamma_{22} & \cdots & & \\ \vdots & \cdots & & \\ \Gamma_{81} & \cdots & & \Gamma_{88} \end{vmatrix}, \dots, \Lambda_{18} = -\begin{vmatrix} \Gamma_{21} & \Gamma_{22} & \cdots & \Gamma_{27} \\ \Gamma_{22} & \cdots & & \\ \vdots & \cdots & & \\ \Gamma_{81} & \cdots & & \Gamma_{87} \end{vmatrix}$$

Thus, the mode shapes of vertical and horizontal bending vibrations of the first shaft segment, (i=1), can be determined as

$$\bar{w}_{1,y}(x) = \Lambda_{11}\cos(\beta^{(1)}x) + \Lambda_{12}\sin(\beta^{(1)}x) + \Lambda_{13}ch(\beta^{(1)}x) + \Lambda_{14}sh(\beta^{(1)}x) \tag{3.6}$$

$$\bar{w}_{1,z}(x) = \Lambda_{15}\cos(\beta^{(1)}x) + \Lambda_{16}\sin(\beta^{(1)}x) + \Lambda_{17}ch(\beta^{(1)}x) + \Lambda_{18}sh(\beta^{(1)}x) \tag{3.7}$$

with $\Lambda_1 = [\Lambda_{11},\ \Lambda_{12},\ \dots\ ,\ \Lambda_{18}]^T$

For the remaining of shaft segments, (i=2,3...n), the eigenvectors, $(\Lambda_2,\ \Lambda_3,\ \dots\ ,\ \Lambda_8)$, can be determined using the relationships given by Eq. (2.46), as follows

$$\begin{aligned} \Lambda_2 &= B_1^{(1)}\Lambda_1, \\ \Lambda_3 &= B_2^{(1)}B_1^{(1)}\Lambda_1, \\ \Lambda_4 &= R_3^{(1)}B_2^{(1)}B_1^{(1)}\Lambda_1, \\ \Lambda_5 &= S_4^{(1)}R_3^{(1)}B_2^{(1)}B_1^{(1)}\Lambda_1, \\ &\vdots \\ \Lambda_n &= B_{n-1}^{(1)} \dots S_4^{(1)}R_3^{(1)}B_2^{(1)}B_1^{(1)}\Lambda_1. \end{aligned} \tag{3.8}$$

3.2 *Forced bending vibrations analysis*

The coefficient vector for forced whirling vibration of the first shaft segment can be determined from Eqs. (3.1) as follows

$$a_1^{(\mu)} = \begin{bmatrix} -D_1^{(\mu)}(0) + \left[j\mu\omega c_0^{(\mu)} - (\mu\omega)^2 \bar{E}M_0 \right] C_1^{(\mu)}(0) \\ \left[-D_n^{(\mu)}(L_n) + (\mu\omega)^2 \bar{E}M_n C_n^{(\mu)}(L_n) \right] B_{n-1}^{(\mu)} \dots\dots B_5^{(\mu)} S_4^{(\mu)} R_3^{(\mu)} B_2^{(\mu)} B_1^{(\mu)} \end{bmatrix}^{-1} \begin{Bmatrix} \bar{E}\bar{f}_0^{(\mu)} \\ 0 \end{Bmatrix}, \mu = 1,2,\dots \tag{3.9}$$

Using the relationships given by equation (2.46), the vectors of constant coefficients $a_2^{(\mu)},\ a_3^{(\mu)}, \dots,\ a_n^{(\mu)}$ can be easily calculated.

4 APPLICATION TO A TYPICAL MARINE PROPELLER SHAFTING SYSTEM

A marine propeller shafting system of a real cargo ship (see figure 3) is considered to calculate the static deformations and the natural frequencies with their associated mode shapes of lateral vibrations. The responses of the system under the first and second blade frequency excitations are also examined. The analysed system consists of a propeller, stepped propeller shaft composed of three shaft segments ((1), (2), and (3)) supported by an anisotropic continuous bearing of Winkler's type, intermediate shaft composed of two shaft segments ((4) and (5)) supported by an anisotropic bearing, a reduction gear supported by two anisotropic bearings and composed of four shaft segments ((6), (7), (8) and (9)), and a thrust bearing. The given data for Figure 5 are as follows:

Young's modulus $E_i = 2.1 \times 10^{11} N/m^2$, and mass density $\rho_i = 7850\ kg/m^3$. The other parameters of the shafts and propeller are provided in Table 1 and Table 2, respectively.

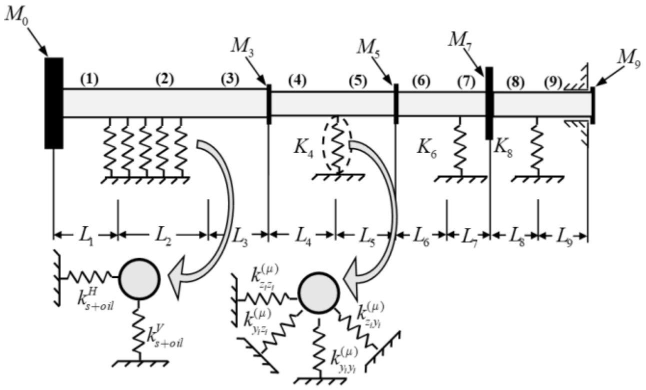

Figure 3. Analysed marine propeller shafting system.

Table 1. The details of marine shafting system.

Length	*L1* *0.840m*	*L2* *3.560m*	*L3* *1.550m*	*L4* *1.650m*	*L5* *4.800m*	*L6* *0.850m*	*L7* *0.970m*	*L8* *0.975m*	*L9* *0.922m*
Diameter	*d1* *0.56m*	*d2* *0.555m*	*d3* *0.565m*	*d4* *0.405m*	*d5* *0.405m*	*d6* *0.420m*	*d7* *0.420m*	*d8* *0.420m*	*d9* *0.420m*
Mass	*m3* *1363.6kg*	*m5* *1363.6kg*							
Diametrical mass moment of inertia	*J3* *82.4109kgm²*	*J5* *82.4109kgm²*							
Intermediate bearing	*k22* *2.56667 x 10⁷N/m*	*k23* *1.64815 x 10⁷N/m*			*k32* *0.32963 x 10⁷N/m*		*k33* *0.89 x 10⁷N/m*		
Reduction gear bearing (propeller side)	*kyy* *1.2613 x 10⁷N/m*				*kzz* *6.8869 x 10⁷N/m*				
Reduction gear bearing (motor side)	*kyy* *1.2223 x 10⁷N/m*				*kzz* *6.5366 x 10⁷N/m*				
Stern tube bearing	*kVoil* *9.37537 x 10⁶N/m²*				*kHoil* *4.49802 x 10⁷N/m²*				

Table 3. Propeller hydrodynamic excitations.

Harmonic of blades	Amplitude and phase of variables hydrodynamic excitations							
	$\bar{f}_{02}^{(\mu)}(N)$	$\varphi_{02}^{(\mu)}$	$\bar{f}_{03}^{(\mu)}(N)$	$\varphi_{03}^{(\mu)}$	$\bar{f}_{05}^{(\mu)}(N.m)$	$\varphi_{05}^{(\mu)}$	$\bar{f}_{06}^{(\mu)}(N.m)$	$\varphi_{06}^{(\mu)}$
μ=1 x z=4	10220	153°	9744	56°	46887	149°	47431	58°
μ=2 x z=8	1173	17°	1917	-66°	7773	2°	12555	-83°
μ=0	Value of constant hydrodynamic excitations							
	$\bar{f}_{02}^{(0)}(N)$		$\bar{f}_{03}^{(0)}(N)$		$\bar{f}_{05}^{(0)}(N.m)$		$\bar{f}_{06}^{(0)}(N.m)$	
	288		12713		1662		119175	

According to pressure measurements on the submerged part of the ship's stern and calculations using lifting surface theory conducted by the shipbuilder, the first and second blade harmonics are considered in this analysis. The propeller hydrodynamic excitations are expressed in the following form

$$f_{0\alpha} = f_{0\alpha}^{(0)} + \sum_{\mu} f_{0\alpha}^{(\mu)} \cos\left(\nu\omega t + \varphi_{0\alpha}^{(\mu)}\right), \quad (\mu = 4,8), \ (\alpha=2, 3, 5, 6)$$

Table 2. Parameters of the propeller.

Parameters	Value
Number of blades	z=4
Mass	m_p=13500kg
Diametrical mass moment of inertia	J_{yy}=9996kgm^2
Polar mass moment of inertia	J_p=19992kgm^2
Nominal speed	Ω =112 rpm
Diameter	D=5.5m

The propeller hydrodynamic excitations are shown in Table 3.

5 NUMERICAL RESULTS AND DISCUSSION

The natural frequencies and associated mode shapes as well as global responses for lateral vibrations of the propulsion shafting system were calculated using a developed computer programs. The natural frequencies and their associated mode shapes are presented in Table 5 and Figures 4-11, respectively.

The major propeller excitations at MPP (Maximum Propulsion Power) are listed in table 4. The rotation speed at MPP is Ω =112 rpm.

Table 4. The major propeller excitations at MPP.

Order	Excitation frequency [rpm]
4. Ω	448
8. Ω	896

Table 5. Natural frequencies of the lateral vibration mode shapes.

Mode shape	Frequency [rpm]	Separation margin (Excitation order)
1st	238	-46,87% (4.Ω)
2nd	365	-18,52%\ (4.Ω)
3rd	561	-37,38% (8.Ω)
4th	758	-15,40% (8.Ω)

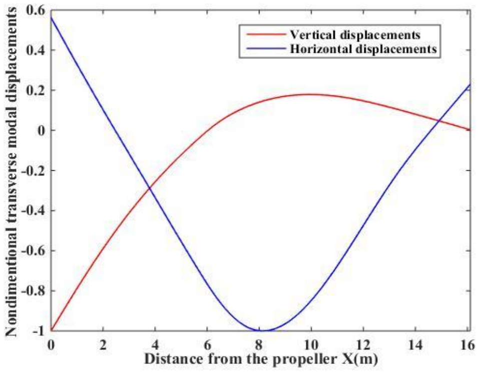

Figure 4. First mode shapes of vertical and horizontal vibrations.

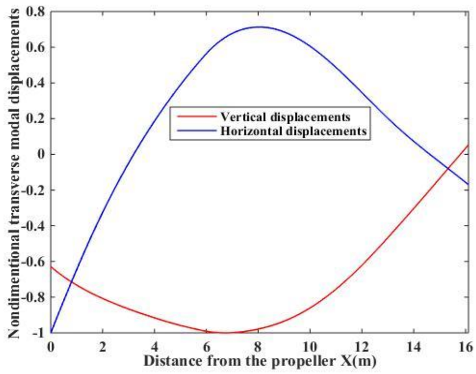

Figure 5. Second mode shapes of vertical and horizontal vibrations.

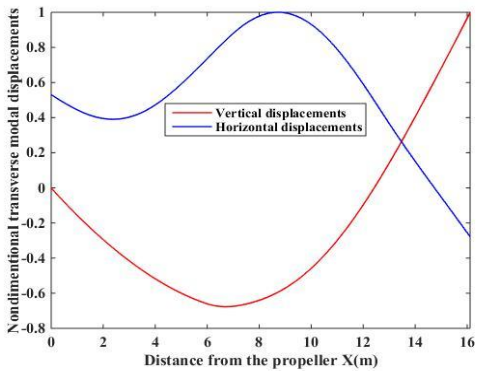

Figure 6. Third mode shapes of vertical and horizontal vibrations.

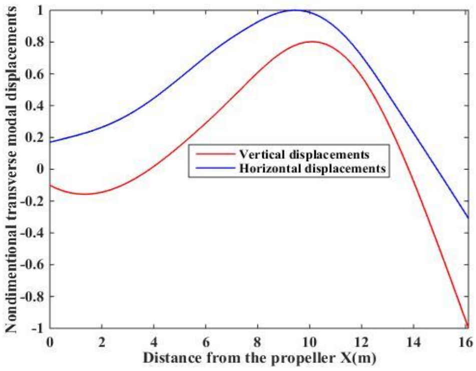

Figure 7. Fourth mode shapes of vertical and horizontal vibrations.

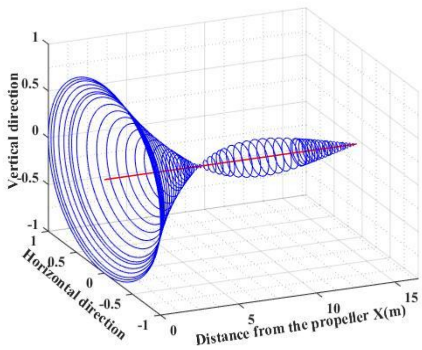

Figure 8. The first whirling mode shape of lateral vibrations.

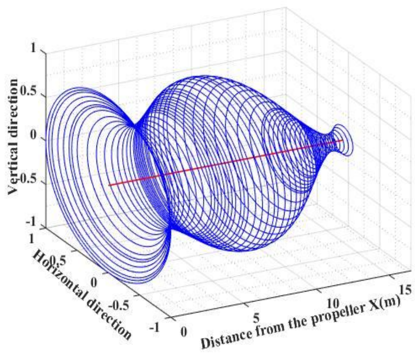

Figure 9. The second whirling mode shape of lateral vibrations.

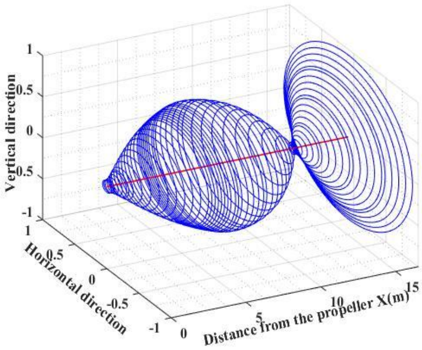

Figure 10. The third whirling mode shape of lateral vibrations.

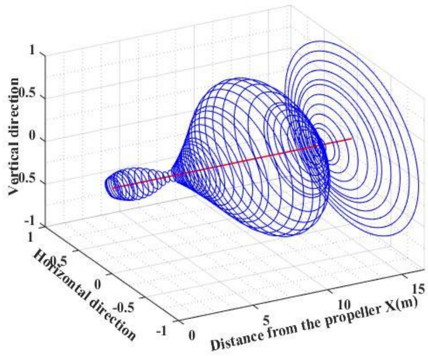

Figure 11. The fourth whirling mode shape of lateral vibrations.

Equations (2.1) and (2.4) were also employed to analyse the deformations caused by the constant components of the propeller excitations (i.e., for μ=0), discarding the ($\frac{\partial^2 w_{i,y}(x,t)}{\partial t^2}$ and $\frac{\partial^2 w_{2,y}(x,t)}{\partial t^2}$) terms and adding the distributed load q_i from the weight of the *i*th shaft segment, to the right-hand side of these equations.

Figure 12 illustrates the static vertical deflection *Y1*(x) caused by the distributed weight of the shaft line, including the propeller and flange couplings. In contrast, Figure 13 depicts the static vertical deflection *Y(x)* induced by the constant components of the propeller excitations. The superposition of both effects is illustrated in Figure 14.

It is concluded that vertical deflection decreases during propulsion system operation due to the constant components of propeller excitations (moment and force).

The decrease at the propeller level (from 6 mm to 5 mm) is crucial for the stern tube bearing's performance, as it decreases unit pressure and influences oil film thickness.

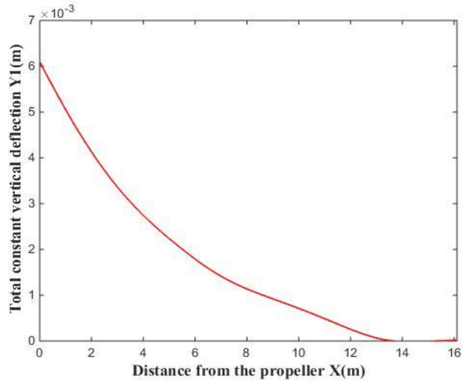

41

Figure 12. Vertical deflection *Y1(x)* due to the distributed weight of the shaft line.

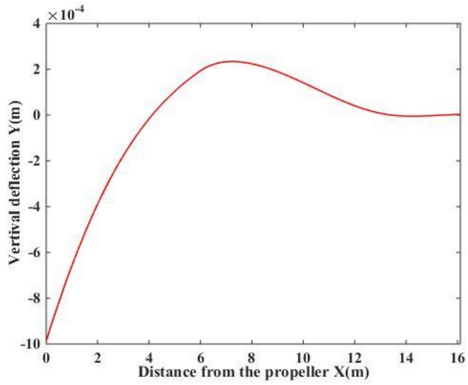

Figure 13. Vertical deflection *Y(x)* due to constant component of propeller excitations.

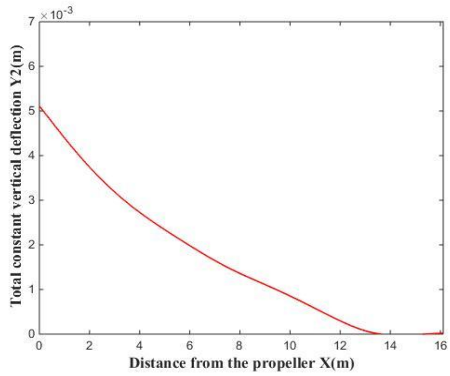

Figure 14. Total vertical deflection *Y2(x)=Y1(x)+Y(x)*

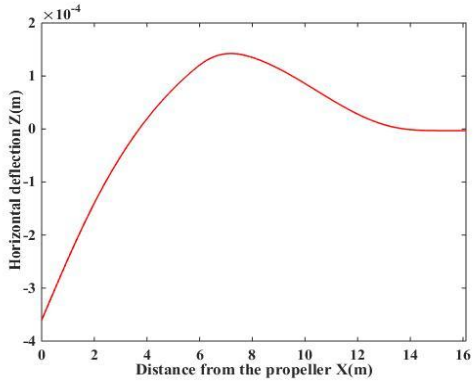

Figure 15. Horizontal deflection Z(x) due to the constant component of propeller excitations.

Figure 15 depicts the horizontal deflection of the propulsion shafting system resulting from the constant components of propeller excitations

Since the separation margins for the second and fourth modes were within 20% of the (4Ω) and (8Ω) excitation frequencies at MPP, an additional harmonic excitation response analysis was conducted to investigate the effect of propeller excitations on the magnitude of the lateral displacement of the shafting system.

The vertical and horizontal vibration amplitudes are plotted in Figures 16 and 17, respectively. The vertical and horizontal displacements at the propeller do not exceed 0.3 mm. Therefore, lateral vibration issues are not expected in the propulsion shafting system under normal operating conditions.

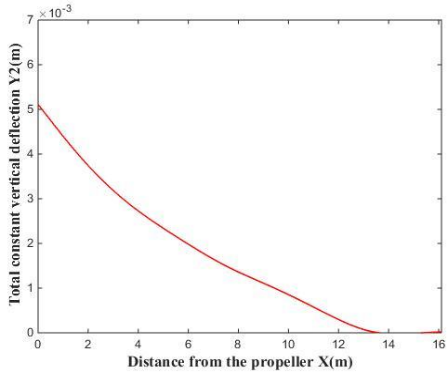

Figure 16. Amplitudes of vertical vibrations.

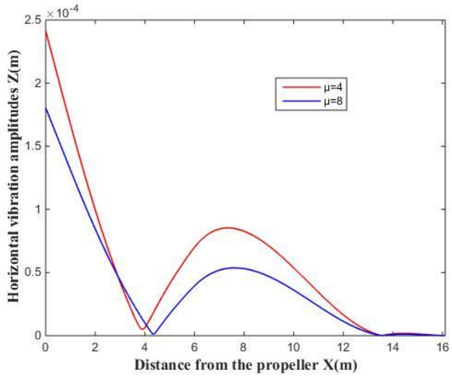

Figure 17. Amplitudes of horizontal vibrations.

6 CONCLUSION

In this work, the matrix formulation of relationships derived from equilibrium and compatibility equations at each junction of adjacent shaft segments enables efficient computation of natural frequencies and lateral whirling vibration amplitudes, considering the propeller's gyroscopic effect, as well as the added mass and damping of seawater.

The constant deflection due to the weight of the shafts, propeller, and flange couplings is significantly greater than the transverse vibration amplitudes in the analysed shaft line.

The constant components of the bending force and moment from the operating propeller can contribute to the straightening of the propeller shaft, reducing the weight-induced deflection of the propeller shaft end by approximately 1 mm in the analysed system, thereby improving the operating conditions of the stern bearing. However, this does not reduce the importance of static calculations in ensuring proper shaft line alignment and uniform load distribution on the radial bearings.

REFERENCES

[1] Batrak, Y., Batrak R., Berin D. 2015. Mikhno A., Propulsion shafting whirling vibration: case studies and perspectives. SNAME 14th Propeller and Shafting Symposium, Norfolk, Virginia, USA, September 2015. Paper Number: SNAME-PSS-2015-002.https://doi.org/10.5957/PSS-2015-002.

[2] Volcy, G. C. 1978. Interaction and Compatibility Between Machinery and Hull from a Static and Vibratory Point of

View. The Society of Naval Architects and Marine Engineers, Ship Vibration Synposium, Arlington, Va., October 16-17,1978.
[3] Bureau Veritas. 2025. BV rules for the classification of steel ships, part C, machinery, electricity, automation and fire protection. Chap. 1, Sec. 9. BureauVeritas, Neuilly-sur-Seine, France, 156.
[4] LIoyd Register of Shipping. 2025. Guidance notes (LR) rules and regulations for the classification of ships. Lloyd's Register, London, UK.
[5] DetNorskVeritas DNV. 2021. Ship Vibration and Noise.Rules for the Ship Classification.
[6] Zou, D., Rao, Z., TA, N. 2016. Coupled longitudinal-transverse dynamics of a marine propulsion shafting under superharmonic resonances. Journal of sound and vibration. 372, 299-316.
[7] Busquier, S., Martinez, S., Legaz, M.J. 2018. Marine propulsion shafting: A study of whirling vibrations. Progress in Maritime Technology and Engineering, 1st Edition, 2018.
[8] Kim, YG., Kim, UK. 2020. Design and analysis of the propulsion shafting system in a ship with single stern tube bearing. J Mar Sci Technol 25, 536–548 (2020).). https://doi.org/10.1007/s00773-019-00659-8.
[9] Huang, Q., Zhang, C., Jin, Y., Yuan C., Yan, X. 2015. Vibration analysis of marine propulsion shafting by the coupled finite element method. Journal of Vibroengineering, Vol. 17, Issue 7, 2015, p. 3392-3403.
[10] Zhang, Y., Xu, W., Li Z., He, J. and Yin, L. 2019. Dynamic Characteristics Analysis of Marine Propulsion Shafting Using Multi-DOF Vibration Coupling Model, Shock and Vibration, Volume 2019 |Article ID 5169156 | https://doi.org/10.1155/2019/5169156
[11] Qin, H., Zheng, H., Wenyuan, Q. and Zhang Z. 2019. Lateral vibration control of a shafting-hull coupled system with electromagnetic bearings journal of Low Frequency Noise, Vibration and Active Control 2019, Vol. 38(1) 154–167.
[12] Murawski, L. 2005. Shaft line alignment analysis taking ship construction flexibility and deformations into consideration. Marine Structures 18 (2005) 62–84.
[13] Murawski, L. 2005. Shaft Line Whirling Vibrations: Effects of Numerical Assumptions on Analysis Results. Marine Technology, Vol. 42, No. 2, April 2005, pp. 53-60.
[14] Myklestad, N. O. 1944. A New Method of Calculating Natural Modes of Vibration of Airplane Wings and Other Types of Beams, J. Aeronaut. Sei., 11, pp. 153-162.
[15] Kandouci, Ch. and Adjal, Y. 2014. Forced Axial and Torsional Vibrations of a Shaft Line Using the Transfer Matrix Method Related to Solution Coefficients. Journal of Marine Science and Application, (2014) 13: 200-205.
[16] Hamdi Cherif, Z., Kandouci, Ch. 2020. Dynamic Characteristics of Multi-disk shaft System Using the Vectors of Solution Coefficients, Journal of Mechanical Engineering. Universiti Teknologi MARA (UiTM), Malaysia, 17(3), 2020, 95-115.
[17] Kandouci, C. 2022. Whirling Analysis of Stepped Timoshenko Shaft Carrying Several Rigid Disks. Journal of Mechanical Engineering. Universiti Teknologi MARA (UiTM), Malaysia,19(2): 97–124.
[18] Kandouci, C, Adjal Y, HamdiCherif, Z, Tayeb, R. 2023. Whirling Analysis of Unbalanced Rotor Using the Vectors of Solution Coefficients. Journal of Vibration and Control. 2024;30(15-16):3659- 3676. doi:10.1177/10775463231198897.
[19] Carlton, J. S. Marine Propellers and Propulsion, 4th Edi.; Butterworth-Heinemann, Elsevier Ltd. Oxford, United Kingdom, 2019; pp. 285-288.
[20] Natanson I., P. Chap. VII. Determinnts. In Short Course in Higher Mathematics; Publishing house Lan, St. Petersburg, 1999; pp: 399-401. (in Russian).